

OPEN ACCESS

Intrinsic high-frequency characteristics of graphene layers

To cite this article: Sungwon Moon *et al* 2010 *New J. Phys.* **12** 113031

View the [article online](#) for updates and enhancements.

You may also like

- [Optimal temporal patterns for dynamical cellular signaling](#)
Yoshihiko Hasegawa
- [Pedestal confinement and stability in JET-ILW ELMy H-modes](#)
C.F. Maggi, S. Saarelma, F.J. Casson *et al.*
- [Microscopic bosonization of band structures: x-ray processes beyond the Fermi edge](#)
Izak Snyman and Serge Florens

Intrinsic high-frequency characteristics of graphene layers

Sungwon Moon¹, Kwangrock Jung², Konggyun Park²,
H Jin Kim^{1,4}, Chang-Won Lee^{3,4}, Chan-Wook Baik^{3,4}
and Jong Min Kim³

¹ School of Mechanical and Aerospace Engineering, Seoul National University, Seoul 151-742, Korea

² School of Electrical Engineering, Seoul National University, Seoul 151-742, Korea

³ Frontier Research Laboratory, Samsung Advanced Institute of Technology, Mt. 14-1, Nongseo-Dong, Giheung-Gu, Yongin-Si 449-712, Korea
E-mail: hjinkim@snu.ac.kr, chang-won.lee@samsung.com and cw.baik@samsung.com

New Journal of Physics **12** (2010) 113031 (10pp)

Received 28 June 2010

Published 16 November 2010

Online at <http://www.njp.org/>

doi:10.1088/1367-2630/12/11/113031

Abstract. The experimental results for the high-frequency transport characteristics (from 0.5 to 110 GHz) of graphene sheets are presented. Samples with graphene sheets of a different number of layers, as well as samples without graphene, were fabricated and compared by their room-temperature radio-frequency (RF) transmission properties. From RF two-port network experiments, the circuit parameters of resistance, inductance and capacitance were extracted using a lumped circuit model that consists of graphene, metal electrodes and contacts. Self-inductance was suppressed with decreasing number of layers, possibly due to minimized interlayer conduction or scattering. The graphene–electrode contact property shows dependence on the number of graphene layers. Our investigation may promote an understanding of the intrinsic graphene characteristics and graphene–electrode contact configuration in passive graphene devices for RF applications.

⁴ Authors to whom any correspondence should be addressed.

Contents

1. Introduction	2
2. Experiments	2
3. Results and discussion	3
4. Conclusions	9
Acknowledgments	10
References	10

1. Introduction

Graphene, the thinnest sheet of carbon-to-carbon networks, has great possibilities in future technologies for electronic and optical devices. The electronic structure of graphene allows excellent electrical transport that can be easily modified by doping or an external electric field [1, 2]. Graphene is quite stable and inert; hence it is possible to prepare large areas that have low defect densities and low electronic scattering rates [3, 4]. Therefore, graphene may serve as an energy-efficient electrode for large-area display and photonic applications. With an appropriate choice of gate dielectrics, it makes a good carrier channel material in transistors for ac current amplification [5].

Single-layer graphene shows minimum conductivity, $\sigma \approx 4e^2/\pi h$, for aspect ratios $W/L \geq 4$, which corresponds to Fano factor $F \approx 1/3$ [6]. The conductivity of graphene approaches $2-12e^2/h$ in the low charge carrier density limit as Fermi energy tends to zero [7]. Mobilities as high as $2 \times 10^5 \text{ cm}^2 (\text{V s})^{-1}$ have been reported in suspended graphene devices [8, 9]. However, recent interest in the electrical properties of graphene has shifted to its ac mode operation because of graphene's extremely low scattering rates and high mobility. Lin *et al* [10] recently demonstrated a field effect transistor operating up to a few tens of gigahertz with an embedded graphene channel. However, until now, more than 50 GHz operation has not been reported, especially for high-frequency radio-frequency (RF) applications.

In this work, we report the high-frequency (from 0.5 to 110 GHz) characteristics of single-, double- and five-layer graphene sheets fabricated by mechanical exfoliation and patterned metal electrodes. Our findings suggest that the impedance of graphene decreases as the layer number increases in the dimension considered here. Self-inductance in the ac mode decreases with decreasing number of layers, possibly due to the lack of inter-layer conduction and scattering centers from π -bonding. The importance of this research lies in understanding the ac mode characteristics of graphene by a comparative study on the effect of the number of graphene layers and their transport characteristics up to 110 GHz.

2. Experiments

Graphene samples were obtained by mechanically exfoliating from HOPG (highly oriented pyrolytic graphite) bulk graphite crystals [11] and deposited onto SiO_2/Si substrate. The thickness of SiO_2 film was 500 nm. The device was designed in order to minimize loss through the substrate typically expected in high-frequency operation. A Renishaw Ramascope 3000 was used for measuring Raman spectra, as shown in figure 3. To avoid irregularities along the

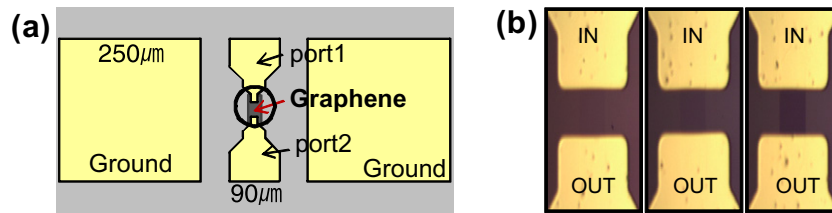


Figure 1. Samples prepared for two-port S -parameter measurements. (a) Schematic drawing of the electrode pattern compatible with GSG probing and graphene sheet. (b) Zoom-in views of the circled region in (a) of each device with monolayer, bilayer and five-layer graphene (left to right), where the electrodes are connected by graphene.



Figure 2. Optical images of graphene samples after the etch process from left to right, monolayer, bilayer and five layers.

edges of graphene and variations in dimensions, we used oxygen plasma etching for generating identical shapes of graphene. Oxygen plasma etching was performed with NEXTRAL NE100 under a condition of 100 sccm oxide and 400 W radio-frequency (RF) power for 2 min.

In order to observe the RF transmission properties of graphene, we fabricated devices compatible with ground–signal–ground (GSG) probing. The devices consist of two contact pads for ground, and IN/OUT electrodes connected by graphene, shown in figure 1(a). The electrodes were patterned by standard photolithography with AZ5214 solution and AZ 300 K for photoresist and developer, respectively. The electrode materials made of Cr/Au bilayer were deposited on SiO_2/Si substrate using e-beam evaporation, and then lifted off in 55 °C acetone solution. The two ground electrodes were $250 \times 250 \mu\text{m}^2$ squares and the IN/OUT electrodes are designed as a tapered shape, their width decreasing from 90 to 31 μm . Identical structures without graphene (called open) and with a rectangular Cr/Au wire of 31 μm width (called thru), respectively, were also fabricated. Figure 1(b) shows the close-up views of the circled region of figure 1(a), where the IN and OUT electrodes are connected by graphene. The effective graphene length (i.e. the gap between the IN and OUT electrodes) is 10 μm .

3. Results and discussion

Graphene sheets are located on top of 500-nm-thick SiO_2 on Si substrate by the standard exfoliation technique [11]. Figure 2 shows the optical images of our graphene samples after the

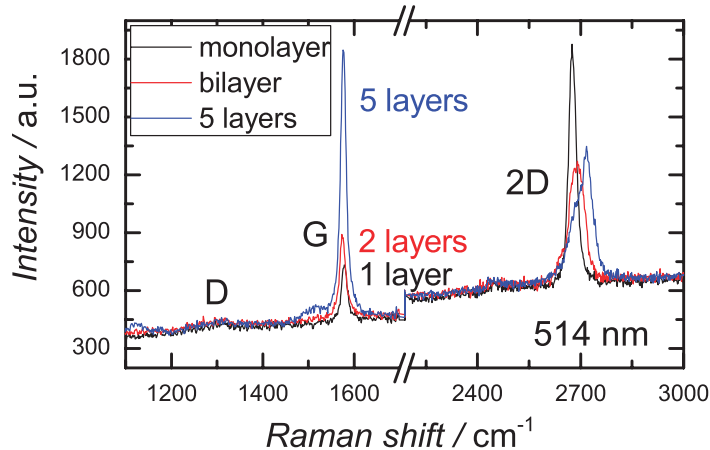


Figure 3. Raman spectroscopy of graphene sheets.

etching process. The graphene sheets are $11 \mu\text{m}$ wide and $31 \mu\text{m}$ long. The number of layers of graphene was identified by optical contrast and Raman spectroscopy. It was reported that the second-order Raman 2D band is sensitive to the number of graphene layers [12, 13]. The 2D band of monolayer graphene is very sharp and symmetric, and for bi- and multilayers it becomes much broader and edgeless because of the change in the electronic structure of graphene. The difference in the 2D band is not obvious for two to four layers. The G band, however, almost linearly increases with the number of layers [13]. Figure 3, the 514 nm Raman spectra of our graphene samples, suggests that samples are monolayer, bilayer and five layers and the ratio of the intensities of the G and 2D peak ($G/2D$) was 0.39, 0.70 and 1.37, respectively.

With deposited graphene samples, we fabricated devices compatible with GSG probing. S -parameters for the samples were measured using a network analyzer (manufactured by Agilent PNA E8361A, at -15 dBm). A standard full two-port calibration using short, open, load, thru configuration was used to de-embed the parasitic effects of the measurement setup. Recent applications and details of the S -parameter technique to analyze RF behavior can be found in studies of single-wall carbon nanotubes [14] and multiwall nanotubes (MWNT) [15].

The reflected electromagnetic wave amplitude (S_{11}) and the transmitted wave amplitude (S_{21}) are plotted in figure 4. As expected, the open configuration shows the largest value of S_{11} , and the thru configuration the smallest. Between them lie the curves for samples A, B and C in order of decreasing magnitude. The order of the S_{21} magnitude is in the reverse order of open–monolayer–bilayer–five layers–thru. Even though the thickness of bilayer graphene is of the order of 1 nm [16], the S_{21} magnitude of the bilayer sample is only 15 dB lower than the sample with 400-nm-thick Au of thru configuration. Note that the width of Au is three times greater than that of samples with graphene. Similar behavior is seen in samples with more layers of graphene. The insertion loss, which is defined as

$$\text{IL} = -10 \log \frac{|S_{21}|^2}{1 - |S_{11}|^2} \text{ dB},$$

is calculated from S -parameter data for each sample, as shown in figure 5. The insertion loss of open configuration shows the greatest value and that of the graphene sample decreases with the number of layers.

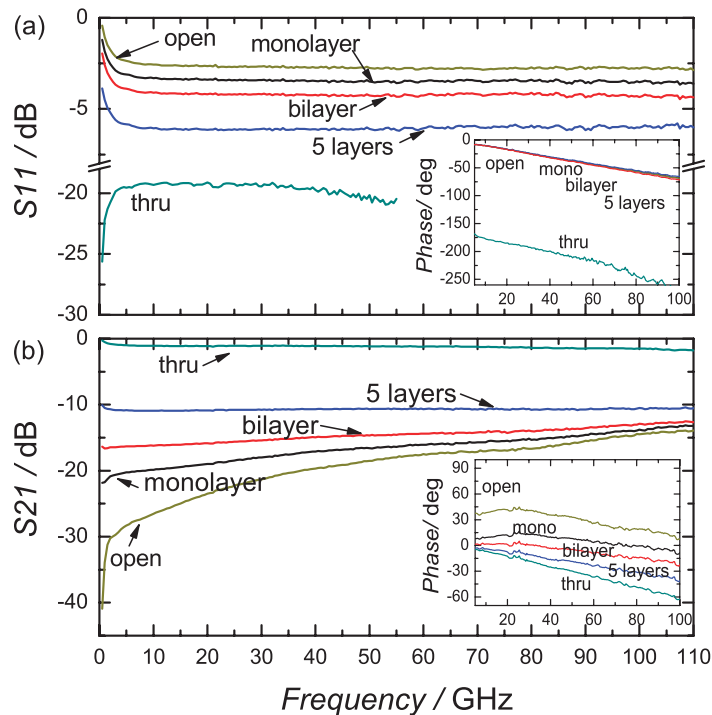


Figure 4. S -parameter data of samples with graphene, and open (without graphene) and thru (10/400-nm-thick Cr/Au wire, $31\ \mu\text{m}$ in width) configurations. (a) S_{11} magnitude (dB) and phase (degree). (b) S_{21} magnitude (dB) and phase (degree).

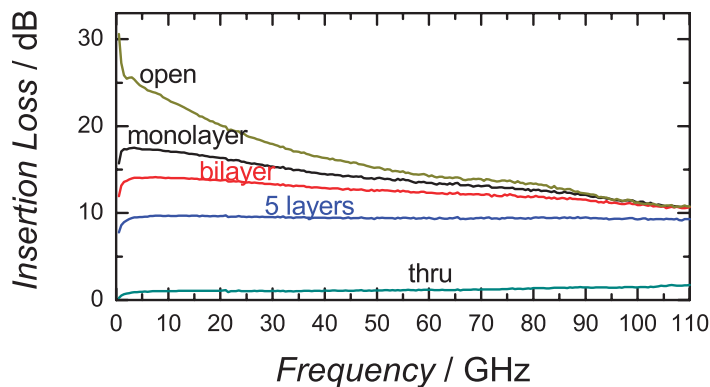


Figure 5. Computed insertion loss with respect to frequency. The insertion losses for samples with graphene are greater than for the thru configuration and increase with decreasing number of layers.

Figure 6 shows a one-dimensional lumped circuit model for samples with graphene sheets. This model successfully explained the RF transport phenomena of the carbon nanotube circuit in previous work [17] and can extract intrinsic parameters of graphene by fitting the experimentally obtained S -parameter data, including the effects of graphene, contact and electrodes separately. R_p and C_p denote the resistance and capacitance of the probing pads and C_{ps} denotes the parasitic

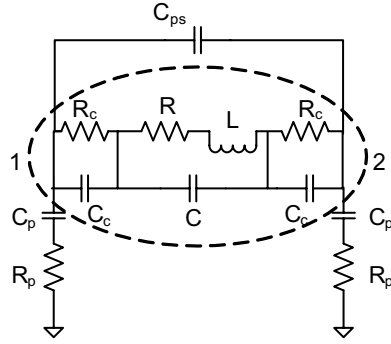


Figure 6. Equivalent lumped circuit model for our graphene device [17]. The dotted circle represents the graphene part. C_p and R_p model the probing pads, C_{ps} denotes the parasitic capacitance of the gap, and R_c and C_c denote the contact resistance and capacitance between graphene and the electrodes. The elements R , L and C represent the graphene sheets.

capacitance of the gap. R_c and C_c denote the contact resistance and capacitance due to the electron transport barriers between the graphene sheet and Cr/Au electrodes. R , L and C are the resistance, inductance and capacitance of the graphene sheet itself, respectively.

By applying the current and voltage law to the circuit model in figure 6, the relationship between the current and the voltage drop between points 1 and 2 can be computed. The frequency-dependent matrix from those points V_1 , V_2 to currents I_1 , I_2 (the so-called Y -matrix, or admittance matrix) can be obtained as follows [17]:

$$\begin{bmatrix} I_1 \\ I_2 \end{bmatrix} = \begin{bmatrix} \hat{Y}_{11} & \hat{Y}_{12} \\ \hat{Y}_{21} & \hat{Y}_{22} \end{bmatrix} \begin{bmatrix} V_1 \\ V_2 \end{bmatrix},$$

$$\hat{Y}_{12}(j\omega) = \hat{Y}_{21}(j\omega) = - \left(\frac{1}{Z(j\omega)} + j\omega C_{ps} \right), \quad (1)$$

$$\hat{Y}_{11}(j\omega) = \hat{Y}_{22}(j\omega) = \left(-\hat{Y}_{21}(j\omega) + \frac{j\omega C_p}{1 + j\omega R_p C_p} \right),$$

where

$$Z(j\omega) = \frac{2R_c}{1 + j\omega R_c C_c} + \frac{R + j\omega L}{(j\omega)^2 LC + j\omega RC + 1} \quad (2)$$

represents the impedance of the graphene sheet, corresponding to the dotted circle in figure 6.

The Y -matrix data [Y_{11} , Y_{12} , Y_{21} , Y_{22}] can be obtained from the measured S -parameter data [S_{11} , S_{12} , S_{21} , S_{22}] using the standard two-port network parameter relationships [18]. By using equations (1) and (2), we fitted the plot of Y_{21} from the data with \hat{Y}_{21} , i.e. we numerically obtained the set of R , L , C , R_c , C_c and C_{ps} values that minimize the error between the data and the circuit model over the frequency range. The error was set to $\sum_{\omega} |Y_{21}(j\omega) - \hat{Y}_{21}(j\omega)|$ for each data set. After the process, the magnitude of difference between Y_{21} and \hat{Y}_{21} was fitted within 3% of $|Y_{21}|$ for each data point. We also fitted the plot of $Y_{11} + Y_{21}$ with $\hat{Y}_{11} + \hat{Y}_{21}$ to extract R_p and C_p values in the same way. If the fitted results of R , L , C , R_c , C_c and C_{ps} are physically

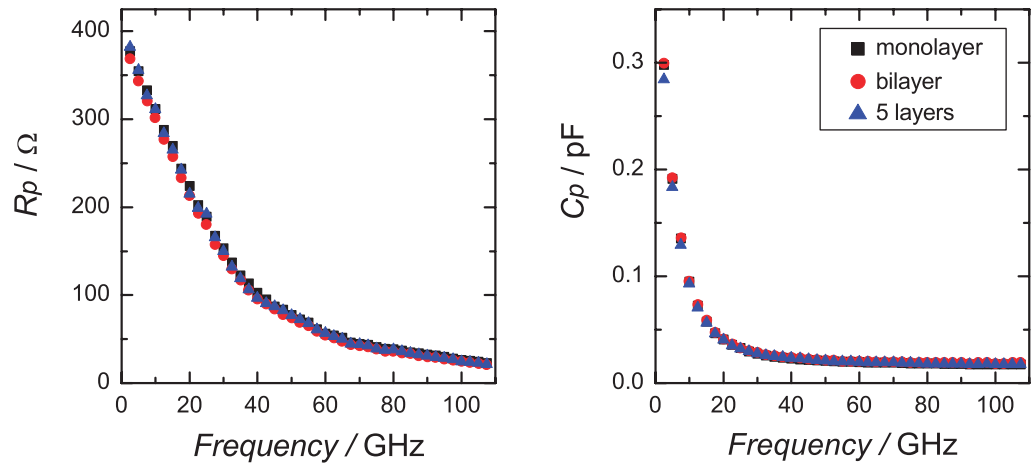


Figure 7. Extracted values of R_p and C_p , which represent the contribution of the metal electrodes. Since all the samples have identical electrode patterns, they show almost identical values regardless of the number of layers.

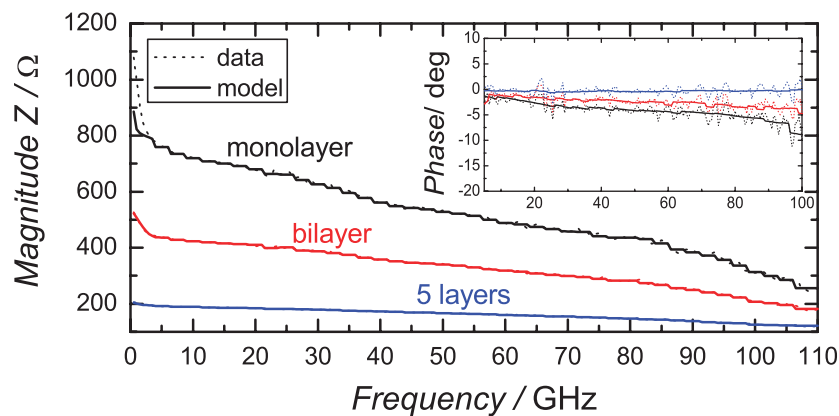


Figure 8. Characteristic impedance Z from the measurement (dotted) and the fitted model (solid): magnitude and phase (inset). The magnitude of $Z(j\omega)$ decreases with increasing frequency, and samples with more layers have smaller impedance.

unreasonable, the resultant fitted values of R_p and C_p for each sample are expected to show uncorrelated behavior. However, as shown in figure 7, R_p and C_p for all three samples show exactly identical features over a wide range of the spectrum, which ensures the quality of the previous fit for R , L , C , R_c , C_c and C_{ps} .

Figure 8 shows the magnitude and phase of the characteristic impedance $Z(j\omega)$ of the graphene samples. The dotted and solid curves are from the raw experimental data and from the fitted model, respectively. The characteristic impedance of graphene itself is in the range of hundreds of ohms. Even though the amplitude of the impedance is reduced from MWNT impedance, the phase of the impedance is still mostly negative, showing capacitive nature similar to MWNT samples [15]. For the single-layer sample, the magnitude decreases drastically from 1000 to 250 Ω with increasing frequency.

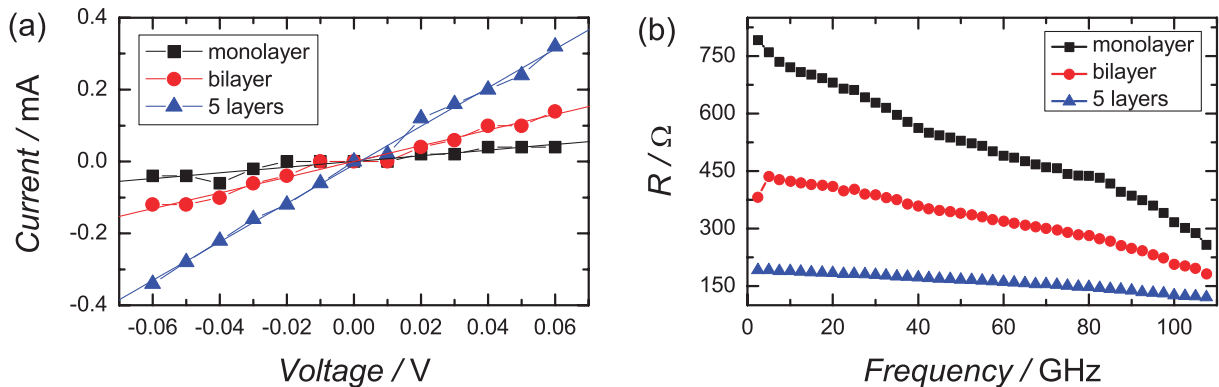


Figure 9. (a) Current–voltage curves (dotted) for each sample with linear fitting (solid). dc resistance values are 1.26 k Ω (monolayer), 0.46 k Ω (bilayer) and 0.19 k Ω (five layers), respectively. (b) Extracted resistance R versus frequency of each graphene. Samples with more layers have smaller resistance R .

The values of R , which are the intrinsic resistances of graphene sheets, are shown in dc I – V characteristics (figure 9(a)) and in ac spectra (figure 9(b)), respectively. The resistances for graphene sheets are of the order of several hundreds of ohms, but notable results can be obtained by comparing the resistances between the samples. For example, at 10 GHz, the R value of monolayer sample is 1.7 and 3.8 times that of bilayer and of five layers, respectively, which are not exactly proportional to the number of layers as reported for dc conductivity [19]. For the complete frequency range, conductivity increases with the number of layers in a sublinear manner. If each layer is assumed to provide the same number of charge carriers, the sublinear increase in conductance implies that the mobility of monolayer graphene is superior to that of any multilayer graphene.

The obtained inductance L generally increases with driving frequency, but the order of magnitudes is very different among the samples, as shown in figure 10(a). Also, the inductive nature of graphene sheets becomes important with increasing number of layers. This inductance enhancement implies that interlayer conduction may become active in the high-frequency region. Therefore, multilayer graphene can be regarded as serially connected conductors with weak scattering centers potentially due to π bondings or crystal lattice misalignments between the layers [20].

The capacitance C of monolayer graphene is of the order of hundreds of attofarads and decreases with more layers, as shown in figure 10(b). The capacitances of both the monolayer sample and the bilayer sample show similar values within experimental error. If only the effect of graphene film thickness is considered, the capacitance of graphene sheets is expected to increase with increasing number of layers. However, as shown in the fitted values, the effect of media such as air or substrate seems more important than the film thickness effect.

For contact between graphene and electrodes, both R_c and C_c increase with respect to number of layers and increasing frequency. As shown in figure 11, in the low-frequency region, R_c is of the order of tens of kilohms and increases up to four times at 100 GHz. C_c is of the order of nanofarads and increases steeply to tens of microfarads at 100 GHz. The enhancements of R_c s are within four times from dc to 110 GHz, while those of C_c s are within four orders of magnitude in the same spectral region. This implies that capacitive coupling between graphene samples and the electrode becomes extremely important in the high-frequency region.

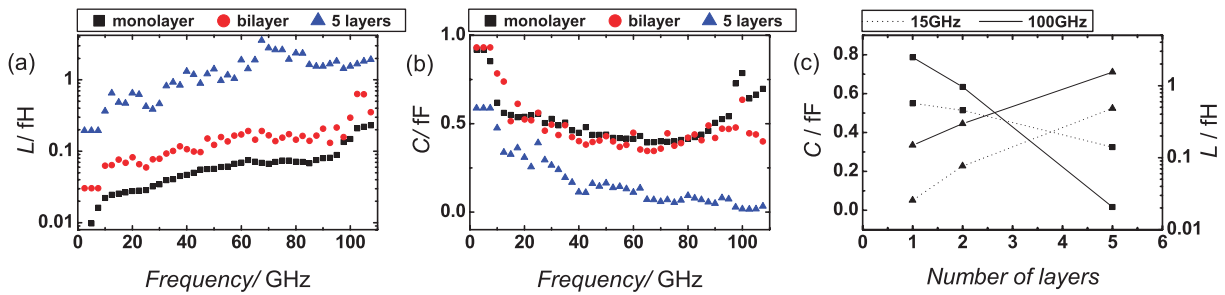


Figure 10. Extracted self-inductance spectra (a) and capacitance spectra (b). Capacitance is of the same order of magnitude for each sample while self-inductance increases dramatically with increasing number of layers as shown in (c). Note that self-inductance is drawn in log scale in (a) and (c). Squares represent the capacitance C and triangles represent the self-inductance L in (c).

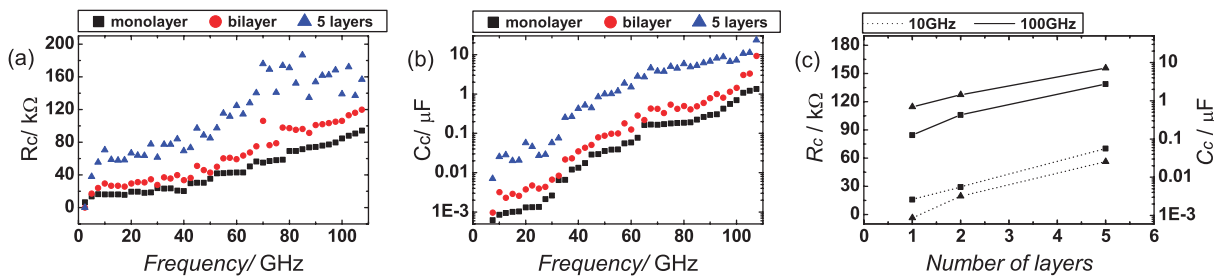


Figure 11. Extracted contact resistance (a) and capacitance (b) from fit. Contact resistances are tens of kilohms and increase up to 200 $k\Omega$. However, contact capacitance increases by four orders of magnitude from 0.5 to 110 GHz, which implies that contact between graphene and electrode becomes extremely important in high-frequency operation. Squares represent the contact resistance R_c and triangles represents the contact capacitance C_c in (c).

R_c decreases with decreasing number of layers, which implies better contact for monolayer graphene. Since the metal electrodes are deposited later on the substrate where the graphene layers have been placed, it is likely that the metal electrodes will contact only with the top layer. Therefore, the increase of C_c with increasing number of layers can result from the bad contact with each graphene layer beneath the top sheet.

Parasitic capacitances C_{ps} show negligible spectral dependence for monolayer and bilayer samples. For five layers, it has characteristic $1/\sqrt{f}$ behavior, which resembles the normal skin-depth effect. Because C_{ps} has generally ten times larger values of intrinsic graphene than C , energy transport through air (by electromagnetic radiation or displacement current) or substrate (by direct current transport) seems more significant in ac mode.

4. Conclusions

In summary, our study supports the structural advantages of single- or double-layer graphene sheet as a channel material for high-frequency RF passive devices operated at room

temperature. Implementing fewer layers of graphene helps reduce the self-inductance possibly originating from interlayer conduction. In order to utilize multiple layers of graphene sheets, further study on the graphene–electrode configuration is required for better contact. In particular, investigations of various edge structures would be necessary because high-frequency transmission characteristics are significantly affected by the graphene edge where atomic structures are broken down.

Acknowledgments

This research has been supported in part by the Ministry of Education, Science and Technology (2010-0027651), Korea and by the Institute of Advanced Aerospace Technology at Seoul National University. The authors thank Dr Seong Chan Jun for help with initial fabrication and equipment-related issues. Measurements were performed in part at Millimeterwave Integrated Systems Lab, Seoul National University.

References

- [1] Castro E V, Novoselov K S, Morozov S V, Peres N M R, Santos J M B L, Nilsson J, Guinea F, Geim A K and Castro Neto A H 2007 *Phys. Rev. Lett.* **99** 216802
- [2] Schedin F, Geim A K, Morozov S V, Hill E W, Blake P, Katsnelson M I and Novoselov K S 2007 *Nat. Mater.* **6** 652
- [3] Li X *et al* 2009 *Science* **324** 1312
- [4] Kim K S, Zhao Y, Jang H, Lee S Y, Kim J M, Kim K S, Ahn J, Kim P, Choi J and Hong B H 2009 *Nature* **457** 706
- [5] Martin J, Akerman N, Ulbricht G, Lohmann T, Smet J H, von Klitzing K and Yacoby A 2008 *Nat. Phys.* **4** 144
- [6] Tworzydło J, Trauzettel B, Titov M, Rycerz A and Beenakker C W J 2006 *Phys. Rev. Lett.* **96** 246802
- [7] Zhang Y, Tan Y W, Stormer H L and Kim P 2005 *Nature* **438** 201
- [8] Bolotin K I, Sikes K J, Ziang Z, Fudenberg G, Hone J, Kim P and Stormer H L 2008 *Solid State Commun.* **146** 351–5
- [9] Morozov S V, Novoselov K S, Katsnelson M I, Schedin F, Elias D C, Jaszczak J A and Geim A K 2008 *Phys. Rev. Lett.* **100** 016602
- [10] Lin Y M, Dimitrakopoulos C, Jenkins K A, Farmer D B, Chiu H Y, Grill A and Avouris P 2010 *Science* **327** 662
- [11] Novoselov K S, Jiang D, Schedin F, Booth T J, Khotkevich V V, Morozov S V and Geim A K 2005 *Proc. Natl Acad. Sci. USA* **102** 10451
- [12] Ferrari A C *et al* 2006 *Phys. Rev. Lett.* **97** 187401
- [13] Graf D, Molitor F, Ensslin K, Stampfer C, Jungen A, Hierold C and Wirtz L 2007 *Nano Lett.* **7** 238
- [14] Plombon J J, O'Brien K P, Gstrein F, Dubin V M and Jiao Y 2007 *Appl. Phys. Lett.* **90** 063106
- [15] Jun S C, Choi J H, Cha S N, Baik C W, Lee S, Kim H J and Kim J 2007 *Nanotechnology* **18** 255701
- [16] Ni Z H, Wang H M, Kasim J, Fan H M, Yu T, Wu Y H, Feng Y P and Shen Z X 2007 *Nano Lett.* **7** 2758
- [17] Jun S C, Huang X M H, Moon S, Kim H J, Hone J, Jin Y W and Kim J M 2007 *New J. Phys.* **9** 265
- [18] Pozar D M 2004 *Microwave Engineering* 3rd edn (New York: Wiley) pp 29–67
- [19] Wang H M, Wu Y H, Ni Z H and Shen Z X 2008 *Appl. Phys. Lett.* **92** 053504
- [20] Ohta T, Bostwick A, McChesney J L, Seyller T, Horn K and Rotenberg E 2007 *Phys. Rev. Lett.* **98** 206802